

## Fluid Mixing from Viscous Fingering

Birendra Jha, Luis Cueto-Felgueroso, and Ruben Juanes\*

*Massachusetts Institute of Technology, 77 Massachusetts Ave, Building 48-319, Cambridge, Massachusetts 02139, USA*

(Received 3 December 2010; published 12 May 2011)

Mixing efficiency at low Reynolds numbers can be enhanced by exploiting hydrodynamic instabilities that induce heterogeneity and disorder in the flow. The unstable displacement of fluids with different viscosities, or viscous fingering, provides a powerful mechanism to increase fluid-fluid interfacial area and enhance mixing. Here we describe the dissipative structure of miscible viscous fingering, and propose a two-equation model for the scalar variance and its dissipation rate. Our analysis predicts the optimum range of viscosity contrasts that, for a given Péclet number, maximizes interfacial area and minimizes mixing time. In the spirit of turbulence modeling, the proposed two-equation model permits upscaling dissipation due to fingering at unresolved scales.

DOI: [10.1103/PhysRevLett.106.194502](https://doi.org/10.1103/PhysRevLett.106.194502)

PACS numbers: 47.51.+a, 47.15.gp, 47.20.Gv, 47.56.+r

Fluid mixing controls many natural and engineered processes, from the ocean biochemistry [1] to population genetics [2] to chemical and biological synthesis in microfluidic devices [3]. Turbulent flows are effective mixers because of the chaotic nature of the velocity field and the aggressive energy cascade spanning a wide range of length scales [4]. Turbulence, however, does not set in at low Reynolds numbers, when inertial effects are negligible. Mixing at low Reynolds numbers, especially in the context of microfluidic applications, has generated a great deal of interest in recent years. Many methods have been proposed to achieve fast mixing in small devices [3], including grooved walls [5], bubble capillary flows [6], pulse injection [7], and acoustic stimulation [8].

All the strategies above assume that the fluids to be mixed have the same viscosity. Here, we investigate how viscosity contrast affects fluid mixing. It is well known that when a less viscous fluid displaces a more viscous fluid, the displacement front is unstable and leads to the formation of a pattern known as viscous fingering [9]. Here we are concerned with the viscous instability of fully-miscible fluids (Fig. 1). The miscible viscous fingering phenomenon has been studied extensively through lab experiments [10,11] and numerical simulations [12–15], yet it is not known how the degree of mixing evolves under viscous fingering and whether optimum mixing can be achieved by varying the viscosity contrast and the flow rate.

Viscous fingering is important in technological applications such as chromatographic separation and enhanced oil recovery from underground reservoirs, in which a low-viscosity fluid is injected to mix with the oil and mobilize it [16]. Recently, it has been shown both theoretically [17] and experimentally [18] that active suspensions of swimming microorganisms may lead to several-fold reduction in fluid viscosity, thereby posing the question of whether biological systems might be naturally exploiting viscous fingering to either promote [19] or arrest [20] mixing.

In this Letter, we characterize the evolution of the degree of mixing between two fluids of different viscosity. We show that viscous fingering leads to two competing effects. On one hand, it enhances mixing by inducing disorder in the velocity field, and increasing the interfacial area between the fluids. On the other, it causes channeling of the low-viscosity fluid, which bypasses large areas of the flow domain—these regions remain unswept thereby reducing the overall mixing efficiency. This competition between creation of fluid-fluid interfacial area and channeling results in nontrivial mixing behavior. We develop a two-equation dynamic model for concentration variance and mean dissipation rate to quantify the degree of mixing in a viscously unstable displacement. The model reproduces accurately the evolution of these two quantities as observed in high-resolution numerical simulations. We then use our analysis to predict the range of viscosity contrast that maximizes mixing.

We consider two-dimensional Darcy flow of a binary mixture. The physical model describes flow in a porous

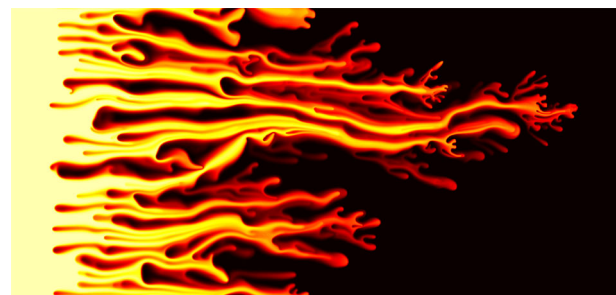


FIG. 1 (color online). Snapshot of the concentration field during the unstable displacement of a more viscous fluid (dark) by a fully-miscible, less viscous fluid (light). The formation, splitting, and nonlinear interaction of viscous fingers induce disorder in the velocity field that affects the mixing rate between the fluids. The displacement corresponds to a viscosity ratio  $M = \exp(3.5) \approx 33$  and Péclet number  $Pe = 10^4$ . See video 1 [26].

medium or Hele-Shaw cell—a thin gap between two parallel plates. We assume that the porosity  $\phi$  (volume of voids per unit volume of porous medium) and permeability  $k$  (coefficient relating flow velocity and pressure gradient) are constant. The two fluids, which are assumed to be first-contact miscible, neutrally buoyant and incompressible, have different viscosity ( $\mu_1 < \mu_2$ ). The diffusivity  $D$  between the fluids is assumed to be constant, isotropic, and independent of concentration. We do not distinguish between longitudinal and transverse diffusivity although it is known that they are different due to hydrodynamic dispersion effects [13]. The length and width of the domain are  $L$  and  $W$ , while the mean velocity is  $U$ . The behavior of the system is governed by two nondimensional groups: the Péclet number  $Pe = UW/D$  and the viscosity ratio  $M = \mu_2/\mu_1$ . A displacement of the high viscosity fluid by the low-viscosity fluid for high mobility ratio and high Péclet number leads to aggressive viscous fingering (Fig. 1) [21]. The governing equations in dimensionless form are

$$\begin{aligned} \partial_t c + \nabla \cdot \left( \mathbf{u}c - \frac{1}{Pe} \nabla c \right) &= 0, & \mathbf{u} &= -\frac{1}{\mu(c)} \nabla p, \\ \nabla \cdot \mathbf{u} &= 0, \end{aligned} \quad (1)$$

in  $x \in [0, L/W]$  and  $y \in [0, 1]$ . The first equation above is a linear advection-diffusion transport equation (ADE) for  $c(\mathbf{x}, t)$ , the concentration, which is 0 for the more viscous fluid and 1 for the less viscous fluid. The second equation is the dimensionless form of Darcy's law, defining the velocity of the mixture, which satisfies the incompressibility constraint. The viscosity of the mixture,  $\mu(c)$ , is assumed to be an exponential function of concentration,  $\mu(c) = e^{R(1-c)}$ , where  $R = \log M$ . Equations are nondimensionalized using characteristic quantities,  $W$ ,  $U$ ,  $P$  and  $\mu_2 = e^R$ , for length, velocity, pressure, and viscosity, respectively. The characteristic time and velocity are given by  $T = \phi W/U$  and  $U = kP/\mu_2 W$ , respectively. In this way, porosity and permeability are absorbed in the definitions of characteristic quantities.

We use the variance of the concentration field to define the degree of mixing,  $\chi$ , as  $\chi(t) = 1 - \sigma^2(t)/\sigma_{\max}^2$ , where  $\sigma^2 \equiv \langle c^2 \rangle - \langle c \rangle^2$  and  $\langle \cdot \rangle$  denotes spatial averaging over the domain. The maximum variance,  $\sigma_{\max}^2$ , corresponds to a perfectly segregated state. In a perfectly mixed state,  $\sigma^2 = 0$  and  $\chi = 1$ . Since viscous fingering instabilities are caused by viscosity contrasts, and therefore by concentration gradients, the decay of  $\sigma^2$  as mixing progresses is closely linked to the decay of the flow disorder due to fingering. Indeed, a natural way to characterize the interplay of mixing and viscous instabilities is to understand the decay of a fully developed fingered flow away from the boundaries. We simulate this flow scenario by considering the mixing of two fluids driven by a constant flow rate in a periodic domain. Initially, the fluids are segregated as a set of irregularly shaped blobs of the more viscous fluid surrounded by the connected, less viscous fluid (Fig. 2).

This flow setup is analogous to that used to study scalar fields in decaying grid turbulence [22]. After a short initial transient, the onset of fingering leads to a highly heterogeneous flow and intense mixing. At later times, the system evolves towards a more homogeneous, synchronous decay of concentration gradients and velocity fluctuations.

In the initial stages of a rectilinear displacement, under a quasi-steady-state approximation (QSSA) of the base state, linear stability analysis predicts the wave number and growth factor of the most unstable mode [23]. In the nonlinear regime, the length scale of viscous fingers arises from diffusion and nonlinear interactions, including channeling, tip-splitting, merging, fading, and shielding [9,13]. The dissipation scale, also referred to as Taylor microscale for the scalar fluctuations [24], is defined in terms of dimensionless quantities as  $s \equiv \sqrt{\sigma^2/\epsilon Pe}$ , where  $\epsilon \equiv \langle |\mathbf{g}|^2 \rangle / Pe$  is the dimensionless mean scalar dissipation rate, and  $\mathbf{g} = \nabla c$ . The scalar dissipation length  $s$  is a transverse length scale in the problem. It is related to the diffusion of scalar gradients across the flow [25], and can be interpreted as the thickness of the interface on which the scalar gradients are localized. The Taylor microscale for mechanical energy is defined as  $\lambda = (\nu u^2/\epsilon_u)^{1/2}$ , where  $\nu$  and  $\epsilon_u$  are the kinematic viscosity and the mean kinetic energy dissipation rate, respectively. At later times, we find the scalings  $\epsilon \sim t^{-2}$ ,  $\sigma^2 \sim t^{-1}$ , and  $s \sim t^{1/2}$ .

Our fundamental insight is the central role played by the scalar dissipation rate,  $\epsilon$ . Multiplying the advection-diffusion equation by  $c$ , averaging over the domain, and using periodicity and incompressibility, we arrive at the evolution equation for the scalar variance [25],

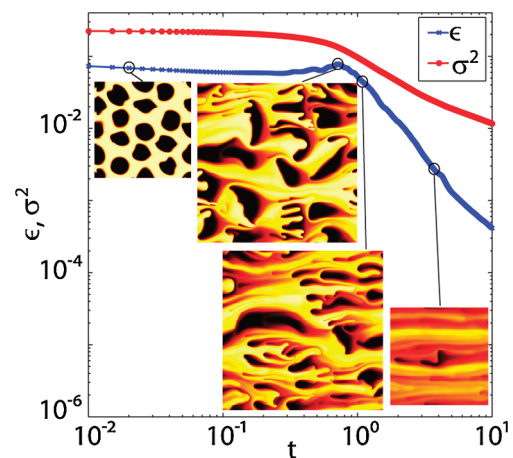


FIG. 2 (color online). Decay of miscible viscous fingering. A binary mixture of initially segregated fluids is driven at constant flow rate in a periodic domain. The variance of concentration,  $\sigma^2$  (red), a proxy for the degree of mixing, decreases monotonically with time. The mean scalar dissipation rate,  $\epsilon$  (blue), increases at early times due to the onset of fingering, and decays monotonically at later times. The simulation parameters are  $R = 2$ ,  $Pe = 10^4$ . See video 2 [26].

$$\frac{d\sigma^2}{dt} = -2\epsilon, \quad (2)$$

which identifies degree of mixing as cumulative dissipation. Physically,  $\epsilon$  can be interpreted as a mixing rate or, equivalently, as a rate at which scalar fluctuations are destroyed. Through interface stretching and tip splitting, viscous fingering increases the scalar dissipation rate and enhances mixing. Since lower viscosity implies higher mobility, fingering also causes channeling of the low-viscosity fluid, which reduces the overall mixing efficiency. The competition between fingering-induced stretching and diffusive forces yields a nonmonotonic evolution of the dissipation rate in time (Fig. 2). The  $\epsilon - t$  curve has a hump at early times, which is a signature of vigorous fingering, and decays monotonically at later times. Heterogeneity and disorder induced by viscous fingering leads to flow fields with statistical properties that resemble those of decaying turbulence (Fig. 3).

We obtain an evolution equation for  $\epsilon$  by taking the gradient of the ADE, performing a dot product with  $\mathbf{g}$  and averaging over the domain (similar to the derivation of  $k$ -epsilon models in turbulence). Using periodicity (valid in fully developed fingering flow) and incompressibility, we arrive at

$$\frac{d\epsilon}{dt} + \frac{2}{\text{Pe}} \langle \nabla \mathbf{u} : \mathbf{g} \otimes \mathbf{g} \rangle = -\frac{2}{\text{Pe}^2} \langle \nabla \mathbf{g} : \nabla \mathbf{g} \rangle, \quad (3)$$

where  $\nabla \mathbf{u}$  is the gradient of the velocity field. The second term in (3) is the rate of stretching of the square norm of concentration gradient  $\mathbf{g}$  and it is negative due to fingering. For a globally chaotic flow with steady or time-periodic velocity fields, it is proportional to  $\langle |\mathbf{g}|^2 \rangle$ . For viscous fingering displacements, where the velocity field is a function of concentration, the dependency on  $\mathbf{g}$  is stronger and there is an additional dependency on the viscosity contrast. From Darcy's equation,

$$\nabla \mathbf{u} = -\mu^{-1} [R \nabla c \otimes \nabla p + \nabla(\nabla p)]. \quad (4)$$

We combine the effect of  $\langle |\nabla(-\nabla p)| \rangle$  and  $\langle R |\nabla c \otimes \nabla p| \rangle$  in (4) because they evolve similarly in time, which we verified with the multidimensional numerical simulations (not shown). Thus,  $\nabla \mathbf{u} \sim -\mu^{-1} [R \nabla c \otimes \nabla p] \sim R \mathbf{u} \otimes \mathbf{g}$ . Further assuming a spatially averaged kinematic viscosity  $\langle \nu \rangle$ , we obtain the scaling relation between scalar dissipation rate  $\epsilon$  and mechanical dissipation rate  $\epsilon_u = 2\langle \nu \nabla^{\text{sym}} \mathbf{u} : \nabla^{\text{sym}} \mathbf{u} \rangle$ ,

$$\epsilon_u \sim 2\langle \nu \rangle R^2 \langle |\nabla c|^2 \rangle \langle \mu^{-2} |\nabla p|^2 \rangle \sim R^2 \text{Pe} \epsilon. \quad (5)$$

This  $\epsilon_u \sim \text{Pe} \epsilon$  behavior is confirmed in the numerical simulations [Figs. 3(a) and 3(b)]. Using (4), the advective term in (3) becomes

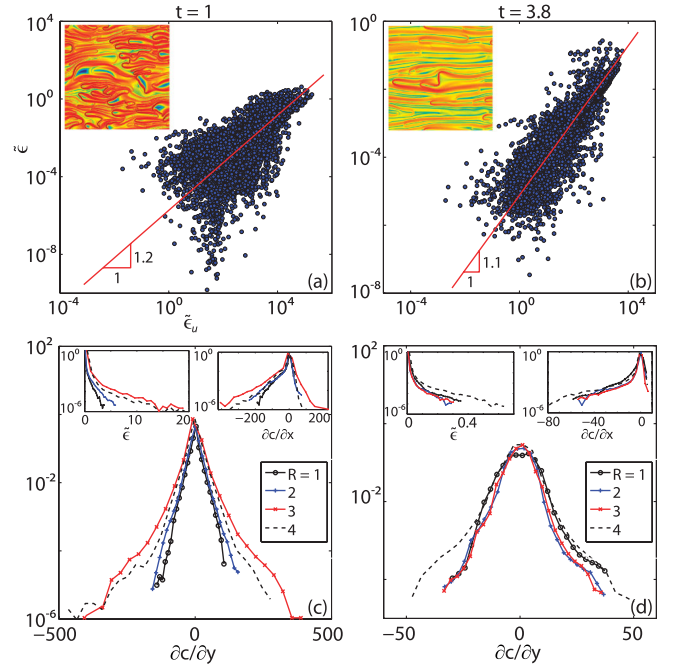


FIG. 3 (color online). The dissipative structure of viscous fingering. (a),(b) The mechanical and scalar dissipation rates synchronize as mixing advances, as shown by the scatter plots of mechanical ( $\epsilon_u$ ) against scalar ( $\epsilon$ ) dissipation rates at early (a) and late (b) times. At late times we find  $\epsilon_u \sim \epsilon^\alpha$ , with  $\alpha \approx 1$ . Inset, logarithm of the scalar dissipation rate. (c),(d) Probability density function (PDF) of the derivatives of the concentration field and scalar dissipation rate. (c) At early times,  $\partial c / \partial y$  exhibits characteristic exponential tails. This behavior is similar to that of passive scalars in turbulent flows [22]. (d) At late times, the PDFs tend toward a Gaussian behavior. The skewness of  $\partial c / \partial x$  reflects the inhomogeneity of the flow.

$$\begin{aligned} \frac{2}{\text{Pe}} \langle \nabla \mathbf{u} : \mathbf{g} \otimes \mathbf{g} \rangle &\sim \frac{2}{\text{Pe}} \langle R |\mathbf{g}|^2 (\mathbf{u} \cdot \mathbf{g}) \rangle \sim -\frac{2R}{\text{Pe}} \langle |\mathbf{g}|^3 \rangle \langle |\mathbf{u}| \rangle \langle \cos \theta \rangle \\ &\sim -R \sqrt{\text{Pe}} e^{-R/4} \frac{\epsilon^{5/2}}{\sigma^2}, \end{aligned} \quad (6)$$

where  $\theta$  is the angle between  $\mathbf{u}$  and  $\mathbf{g}$  vectors at the interface, and we take  $\langle \cos \theta \rangle = e^{-R/4} \epsilon / \sigma^2$ , a model that agrees well with simulations (not shown). The effect of channeling at higher  $M$  is to reduce  $\langle |\mathbf{g}| \rangle$  (by reducing total interfacial area) and realign the gradient vector to become orthogonal to the velocity vector. This realignment reduces  $\langle \cos \theta \rangle$ . Using the ADE,

$$\frac{2}{\text{Pe}^2} \langle \nabla \mathbf{g} : \nabla \mathbf{g} \rangle \sim 2 \langle (\partial_t c + \mathbf{u} \cdot \mathbf{g})^2 \rangle \sim \sqrt{R \text{Pe}} e^{-R/4} \left( \frac{\epsilon}{\sigma} \right)^{5/2}, \quad (7)$$

where we model  $\langle (\partial_t c)^2 \rangle \sim \frac{1}{\sigma^2} \left( \frac{d\sigma^2}{dt} \right)^2 \sim \frac{\epsilon^2}{\sigma^2}$ , and  $-\langle \partial_t c (\mathbf{u} \cdot \mathbf{g}) \rangle \sim \langle (\mathbf{u} \cdot \mathbf{g})^2 \rangle \sim \text{Pe} \epsilon \langle \cos^2 \theta \rangle$ . In a purely diffusive setting ( $R = 0$ ), the evolution of mean dissipation rate, and therefore mixing, also involves interactions among the various interfaces in the domain. The evolution of the interface thickness and  $\epsilon$  transitions from power-law to exponential to an error-function-like behavior in time, with

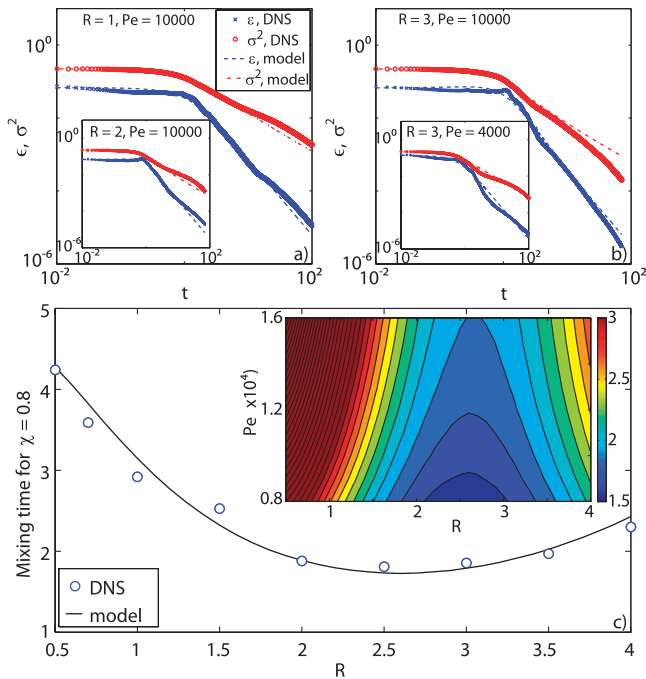


FIG. 4 (color online). (a),(b) The mean dissipation rate (blue) and variance (red) predicted by the two-equation model (dashed) compare well with the results from direct numerical simulations (solid). (c) Mixing time, that is, time to reach 80% degree of mixing, plotted for different mobility contrasts and  $Pe = 10^4$ , from both simulations and the  $\sigma^2 - \epsilon$  model. Mixing time behaves nonmonotonically with  $R$ , increasing at high  $R$  due to channeling. Inset: mixing time surface from the model as a function of  $R$  and  $Pe$ :  $A = 0.76$ ,  $B = 0.84$ .

transition times depending on the initial configuration of the fluid interfaces. Here, we have chosen to model  $R > 0.5$  and  $Pe > 5000$  to avoid dealing with a separate model under pure diffusion. The resulting model equation for  $\epsilon$  is

$$\frac{d\epsilon}{dt} - AR\sqrt{Pe}e^{-R/4}\frac{\epsilon^{5/2}}{\sigma^2} + B\sqrt{RPe}e^{-R/4}\left(\frac{\epsilon}{\sigma}\right)^{5/2} = 0. \quad (8)$$

Equations (2) and (8) form a coupled system of first-order ODEs which can be solved with initial values of  $\sigma^2$  and  $\epsilon$ . This two-equation model is analogous to the  $k$ -epsilon models in turbulence. Equation (8) has two terms corresponding to fingering-induced enhancement and diffusion-driven decrease in the dissipation rate. The advection-driven term is negative and gives the rising behavior in  $\epsilon$  whereas the diffusion-driven term is positive and gives the declining behavior in  $\epsilon$ .

We test the above model predictions by comparing the predicted decay of variance and scalar dissipation rate with results from the direct numerical simulations (Fig. 4). Mixing times predicted from the model compare well with those obtained from the simulations, reaching a minimum around  $R = 2.5$ . Channeling of the less viscous fluid is persistent at high  $Pe$ , as shown by the surface of mixing time as a function of mobility ratio and  $Pe$  [Fig. 4(c)].

Our results show that interfacial area and dissipation rate are the central variables to understand mixing enhanced by viscous fingering. The viscosity contrast that provides optimum mixing time depends on the Péclet number, and arises from a delicate balance between interface stretching due to flow disorder, and channeling due to the higher mobility of the less viscous fluid. The use of ideas from turbulence modeling, synthesized in our two-equation model, provides a framework to upscale the dissipative effects of fingering in large-scale flow models.

Funding for this research was provided by Eni S.p.A. and by the ARCO Chair in Energy Studies.

\*juanes@mit.edu

- [1] K. Katija and J. O. Dabiri, *Nature (London)* **460**, 624 (2009).
- [2] K. S. Korolev, M. Avlund, O. Hallatschek, and D. R. Nelson, *Rev. Mod. Phys.* **82**, 1691 (2010).
- [3] H. A. Stone, A. D. Stroock, and A. Ajdari, *Annu. Rev. Fluid Mech.* **36**, 381 (2004).
- [4] B. I. Shraiman and E. D. Siggia, *Nature (London)* **405**, 639 (2000).
- [5] A. D. Stroock *et al.*, *Science* **295**, 647 (2002).
- [6] P. Garstecki *et al.*, *Lab Chip* **6**, 207 (2006).
- [7] I. Glasgow and N. Aubry, *Lab Chip* **3**, 114 (2003).
- [8] T. Frommelt *et al.*, *Phys. Rev. Lett.* **100**, 034502 (2008).
- [9] G. M. Homsy, *Annu. Rev. Fluid Mech.* **19**, 271 (1987).
- [10] J.-D. Chen, *Exp. Fluids* **5**, 363 (1987).
- [11] P. Petitjeans, C.-Y. Chen, E. Meiburg, and T. Maxworthy, *Phys. Fluids* **11**, 1705 (1999).
- [12] C. T. Tan and G. M. Homsy, *Phys. Fluids* **31**, 1330 (1988).
- [13] W. B. Zimmerman and G. M. Homsy, *Phys. Fluids A* **3**, 1859 (1991).
- [14] C. Y. Chen and E. Meiburg, *J. Fluid Mech.* **371**, 233 (1998).
- [15] M. Mishra, M. Martin, and A. DeWit, *Phys. Rev. E* **78**, 066306 (2008).
- [16] F. M. Orr, Jr and J. J. Taber, *Science* **224**, 563 (1984).
- [17] Y. Hatwalne, S. Ramaswamy, M. Rao, and R. A. Simha, *Phys. Rev. Lett.* **92**, 118101 (2004).
- [18] A. Sokolov and I. S. Aranson, *Phys. Rev. Lett.* **103**, 148101 (2009).
- [19] A. Sokolov, R. E. Goldstein, F. I. Feldchtein, and I. S. Aranson, *Phys. Rev. E* **80**, 031903 (2009).
- [20] K. R. Bhaskar *et al.*, *Nature (London)* **360**, 458 (1992).
- [21] To gain numerical stability at high  $M$ , we solve the system of PDEs in (1) directly, instead of using the stream function vorticity approach [12]. We solve the pressure equation using a two-point flux approximation, and the concentration equation using sixth-order compact finite differences and third-order Runge-Kutta time-stepping.
- [22] Z. Warhaft, *Annu. Rev. Fluid Mech.* **32**, 203 (2000).
- [23] C. T. Tan and G. M. Homsy, *Phys. Fluids* **29**, 3549 (1986).
- [24] V. Eswaran and S. B. Pope, *Phys. Fluids* **31**, 506 (1988).
- [25] S. B. Pope, *Turbulent Flows* (Cambridge University Press, Cambridge, England, 2000).
- [26] See supplemental material at <http://link.aps.org/supplemental/10.1103/PhysRevLett.106.194502>.